Eur. Phys. J. D **1**, 303–311 (1998)

THE EUROPEAN PHYSICAL JOURNAL D

Ionization of metal clusters by ions in the Fermi velocity range

P.G. Reinhard[1], E. Suraud[2,a,b], and C.A. Ullrich[3]

[1] Institut für Theoretische Physik, Universität Erlangen, Staudtstr. 7, 91058 Erlangen, Germany
[2] Laboratoire de Physique Quantique, Université Paul Sabatier, 118 route de Narbonne, 31062 Toulouse Cedex, France
[3] Department of Physics, University of Missouri, Columbia, Missouri 65211, USA

Received: 28 July 1997 / Received in final form: 23 December 1997 / Accepted: 8 January 1998

Abstract. We simulate excitation of metal clusters by highly charged, energetic ions, analyzing electron emission in terms of discrete ionization probabilities. Our test case is the collision of Ar^{8+} on the cluster Na_9^+ at velocities around the electronic Fermi velocity of bulk sodium. The calculations are performed with a density-functional approach, using the time-dependent local density approximation. We find that ionization takes place on an extremely short time scale of less than 5 fs. The preferred final charge state depends sensitively on the impact parameter. High ionization can easily be achieved in sufficiently close collisions. Direct trapping through the by-passing ion is found to be of little importance at the velocities considered.

PACS. 36.40.Cg Electronic and magnetic properties of clusters – 36.40.Wa Charged clusters – 36.40.Gk Plasma and collective effects in clusters

1 Introduction

Highly charged metal clusters have gained considerable interest in recent time [1]. A number of experimental studies investigate Coulomb dissociation of these systems, mainly in terms of critical sizes of stability [2–4]. However, the mechanisms governing the fragmentation processes strongly depend on the conditions under which the high charge states were prepared. For example, conventional techniques using nanosecond laser pulses [2,3] inevitably heat up the cluster, leading to thermally excited systems in which evaporation of neutral atoms competes with fission decay. A "cleaner" way of charging the cluster is thus often desirable. One possible technique uses impact with fast, sometimes highly charged, ions [4]. These collision processes take place on a femtosecond time scale and leave the vibrational state of the cluster essentially unchanged. This leads to shifts of the stability threshold towards higher charge-mass ratios than those which can be achieved with conventionally laser-ionized clusters.

A complete theoretical description of these energetic collision processes in principle calls for the full time-dependent Schrödinger equation for the many-body system, a formidable task which necessarily requires some approximations. The most simple approach at a microscopic level is time-dependent Hartree-Fock [5], which relies on the assumption of independent particle motion in a common mean field. However, many-fermion systems are characterized by strong interparticle correlations, which makes a straightforward Hartree-Fock approach in general too inaccurate. The way out of this dilemma is to account for correlations by means of a local effective potential which then can safely be used in connection with an effective time-dependent Hartree approach. We thus come into the realm of time-dependent density functional theory (TDDFT) [6–8], which we are going to employ here for a study of the collision dynamics in metal clusters. TDDFT is frequently invoked as a computationally efficient tool for studying the dynamics of many-body systems. In actual calculations, one usually works within the time-dependent local density approximation (TDLDA) [6]. Apart from being physically more sound and quantitatively more accurate than semiclassical approaches such as Vlasov [9,10] or hydrodynamics, TDDFT has the additional advantage that it allows one to compute more detailed information on the collision process: using the time-dependent Kohn-Sham (TDKS) single-particle orbitals as input, approximate probabilities for each discrete final charge state of the system can be deduced. Hence, direct contact with experimental data can be established.

Previous applications of TDDFT to sodium clusters [11–13] have demonstrated an overwhelming dominance of the plasmon resonance over the whole investigated range of excitation energies high into the multi-plasmon regime. Those large-amplitude plasmon oscillations may be accompanied by strong electron emission, which leaves the system in a highly charged state, thus providing a seed for fragment formation or even Coulomb explosion at later times [1]. In a recent work we have investigated the global properties of electron emission following a strong and

[a] Membre de l'Institut Universitaire de France
[b] e-mail: suraud@irsamc2.ups-tlse.fr

instantaneous excitation, idealizing a fast ion passing by [14]. It is the aim of this paper to carry through a more realistic and detailed analysis for the case of Na_9^+ clusters excited by fast Ar^{8+} ions. In the following, we are going to employ a detailed description of the collision process in terms of ion probabilities and analyze also the temporal and spatial structure of the electron cloud in order to obtain more information on the nature of the ionization mechanism. We mention that related work has recently been published in [15,16], using femtosecond laser pulses rather than fast ions to ionize the cluster.

The paper is outlined as follows: In Section 2, we give a short record of the ingredients entering our TDLDA calculations of the electronic dynamics (Sect. 2.1) and the excitation process (Sect. 2.2). In Section 3, we describe the way to compute the ionization probabilities from the TDLDA. Results on ionization probabilities are then discussed in Section 4. Finally, in Section 5 we focus on the mechanism of ionization, in particular in terms of electron trapping by the by-passing ion.

2 The model

2.1 Ionic background and valence electrons

The violent excitations of clusters which we are going to consider, last for such a short time (typically up to $t \leq$ 100 fs) that, to a very good approximation, ions can be considered as fixed during that time. At high excitation energy, details of the ionic structure seem furthermore to play only a minor role in the electron response [11]. We thus treat the ionic background in jellium approximation, using a soft jellium surface, which is crucial to reproduce the experimental plasmon resonance energy (2.62 eV for our test case Na_9^+) in a TDLDA calculation [17,18].

The electrons are treated in TDDFT. They are represented by single-particle orbitals $\phi_j(\mathbf{r},t)$ satisfying the TDKS equations. For the exchange-correlation (xc) potential we use the TDLDA with the parametrization of Gunnarsson and Lundqvist [19]. The TDLDA is local both in space and time, *i.e.* the xc potential $v_{\rm xc}^{\rm TDLDA}(\mathbf{r},t)$ only depends on the values of the electron density $n(\mathbf{r},t) = \sum_{j=1}^{N} |\phi_j(\mathbf{r},t)|^2$ at time t and location $\mathbf{r}$. This approximation can be expected to be good only if the time dependence of the process under study is sufficiently slow. In practice, however, it was shown to give quite good results even for cases of rather rapid time dependence [20]. A more detailed description of our procedure and applications to cluster physics is given in [13].

2.2 Excitation through a by-passing ion

We deal with excitations through energetic, possibly highly charged ions passing by at a distance b from the center of the cluster. We restrict ourselves to situations where the projectile stays well outside the cluster bounds (beyond $\sim 10\,a_0$ for our test case Na_9^+) so that only its long-range Coulomb potential needs to be taken into account. In other words, we consider impact parameters b ranging from grazing collisions ($b \sim 10\,a_0$) to very peripheral ones ($b \geq 35\,a_0$). Such excitations deliver to the cluster a very short electromagnetic pulse covering all spectral states with about equal weight. Feedback of the interaction on the exciting ion can, in turn, safely be neglected for massive ions at high velocity. We thus assume that the ionic trajectory itself is not perturbed by the field of the cluster [10]. Furthermore, the retarded parts of the electromagnetic interaction are disregarded, as the velocity of the ion is small as compared to the speed of light. For simplicity, the calculations are performed on an axially symmetric grid (for details of the model see [11,13]), and we orient the z-axis of the coordinate system (with the origin at the center of the jellium distribution) at each time t towards the current position of the projectile. The approximation (which turns out to be reasonable [10]) hence consists in neglecting the axial symmetry breaking in the scattering geometry, so that the cluster effectively sees a cylindrically symmetric time-dependent external potential

$$V_{\rm ion}(\rho,z,t) = \frac{-Q}{\sqrt{\rho^2 + (z-d(t))^2}}, \qquad (1)$$

where ρ and z denote the radial and z component of the cylindrical coordinates. Here, Q is the charge of the ionic projectile with velocity v, and $d(t) = \sqrt{b^2 + v^2(t-t_0)^2}$ is its distance to the cluster's center of mass. The instant of closest approach is set to be at $t_0 = 0$. However, the actual computation starts at an earlier time, $t_0 - \Delta t$, where the ion is still far away, safely before the ion-cluster interaction plays a role. Through variation of the impact parameter b, velocity v and charge Q, the excitation amplitude may be tuned. Here we will consider the highly charged Ar^{8+} ion with velocities $v = 12.5$, 25 and $50\,a_0$/fs, *i.e.* approximately $0.5v_{\rm F}$, $v_{\rm F}$ and $2v_{\rm F}$, where $v_{\rm F}$ is the electronic Fermi velocity in bulk sodium. The corresponding values of Δt are chosen such that the initial distances between the projectile and the cluster are safely large (well beyond 100 a_0).

A few words are in order about the nature of this excitation process [14]. We consider here a situation where the final state of the ion is not measured with high precision. It thus can be assumed that the ion moves on a mean trajectory (which moreover is not affected by feedback from the collision). This means that the ion becomes a strictly classical source of a time-dependent external field. It transfers a certain average excitation energy $\overline{E^*}$, but induces also a substantial energy uncertainty $\Delta E^* \approx \sqrt{\overline{E^*}}$ into the electronic state of the cluster. As a result, final states with different degrees of ionization can arise. The probabilities of their appearance will be discussed in Section 3.

A further property of the external field (Eq. (1)) is that the effective reaction time is extremely short, of the order of $2R/v$ (where R is the cluster radius), which for the cases we consider is typically below the time scale of one plasmon oscillation of Na_9^+ (1.5 fs). The excitation hence essentially amounts to an almost instantaneous acceleration of the electron cloud as a whole. Such a simplistic picture

had been successfully employed in previous exploratory calculations [11–14]. A competing process, however, is the immediate trapping of electrons by the huge attractive field of the ion, which might occur in the case of very close collisions and if sufficient time for a direct electron transfer is available. We will show later that this trapping process is less important than dipole-induced emission, for the fast collisions which we investigate here (see Sect. 5).

3 Calculation of ionization probabilities

The description of electron escape within TDDFT relies on the basic relation

$$N(t) = \int_{\mathcal{V}} \mathrm{d}^3\mathbf{r}\, n(\mathbf{r},t) \tag{2}$$

which associates the number of bound electrons $N(t)$ with the time-dependent density $n(\mathbf{r},t)$ found within the finite volume $\mathcal{V}$ of an "analyzing box" centered around the ionic background. In our calculations, $\mathcal{V}$ consists of a cylinder of length 32 a_0 and radius 16 a_0. From $N(t)$ one can calculate the total number of escaped electrons as $N_{\mathrm{esc}}(t) = N(t{=}-\infty) - N(t)$. Equation (2) is based on the assumption that the electron flux crossing the boundary of this analyzing box corresponds to that part of the total time-dependent wave function which is in the continuum. We hence assume that all important bound-state contributions to the density are contained inside the analyzing box $\mathcal{V}$, whereas the continuum contributions are outside. Strictly speaking, such a criterion is meaningful only after long times, when the continuum contributions have propagated very far away from the center. Nevertheless, equation (2) has proven to be a useful definition of the bound-state occupation probability in a number of applications involving atoms in strong fields [20–23].

A detailed link with experiments is established through probabilities $P^k(t)$ of finding the excited clusters in one of the possible charge states k to which they can ionize. It is possible to write down explicit expressions for the $P^k(t)$ in terms of bound-state occupation probabilities $N_j(t)$ associated with the single-particle KS orbitals ϕ_j,

$$N_j(t) = \int_{\mathcal{V}} \mathrm{d}^3\mathbf{r}\, n_j(\mathbf{r},t) = \int_{\mathcal{V}} \mathrm{d}^3\mathbf{r}\, |\phi_j(\mathbf{r},t)|^2. \tag{3}$$

Note that the ϕ_j (which we shall label in the following by their initial quantum numbers), as well as their orbital densities n_j, have, strictly speaking, no rigorous physical meaning in TDDFT. One should therefore consider the $P^k[\{n_j\}](t)$ deduced from them only as a reasonable approximation to the exact probabilities.

Let us now discuss how one can obtain the $P^k[\{n_j\}](t)$'s from the N_j's. We start with the simple example of a system which at $t = 0$ has only one doubly occupied orbital, such as the helium atom [20,21] or a Na_2 cluster in a spherical jellium model. In this simple case, the $P^k(t)$ are, in fact, explicit functionals of the total density. If the bound-state occupation probability (Eq. (3)) for these systems is given by $N_{1\mathrm{s}}(t)$, then the probabilities for the possible charge states are $P^{(0)}(t) = N_{1\mathrm{s}}(t)^2$, $P^{(1+)}(t) = 2N_{1\mathrm{s}}(t)(1 - N_{1\mathrm{s}}(t))$, $P^{(2+)}(t) = (1 - N_{1\mathrm{s}}(t))^2$. These expressions have been constructed to fulfill the requirement that the probabilities must sum up to unity. The square in $P^{(0)}$ and $P^{(2+)}$ and the factor of 2 in $P^{(1+)}$ account for the degeneracy, as we work with a spin-unpolarized system.

To generalize the above considerations, we start with the relation

$$1 = \prod_j (N_j + (1 - N_j))^{\nu_j} = \prod_j (N_j + \bar{N}_j)^{\nu_j}, \tag{4}$$

where ν_j is the j-orbital degeneracy ($\nu_{1\mathrm{s}} = \nu_{1\mathrm{p}_0} = 2$, $\nu_{1\mathrm{p}_1} = 4$, for unpolarized Na_9^+). Note that the time-dependent orbitals keep their initial degeneracy for the present, spin-independent excitation mechanism (Eq. (1)). We then perform the multiplication on the right-hand side of equation (4) and sort the resulting terms according to the number of occupied and unoccupied orbitals (factors N_j and $\bar{N}_j = 1 - N_j$, respectively). We thus obtain for Na_9^+:

$$P^{(1+)}(t) = N_{1\mathrm{s}}^2 N_{1\mathrm{p}_0}^2 N_{1\mathrm{p}_1}^4 \tag{5}$$

$$\begin{aligned} P^{(2+)}(t) = {} & 4N_{1\mathrm{s}}^2 N_{1\mathrm{p}_0}^2 N_{1\mathrm{p}_1}^3 \bar{N}_{1\mathrm{p}_1} + 2N_{1\mathrm{s}}^2 N_{1\mathrm{p}_0} \bar{N}_{1\mathrm{p}_0} N_{1\mathrm{p}_1}^4 \\ & + 2N_{1\mathrm{s}} \bar{N}_{1\mathrm{s}} N_{1\mathrm{p}_0}^2 N_{1\mathrm{p}_1}^4 \end{aligned} \tag{6}$$

$$\begin{aligned} P^{(3+)}(t) = {} & 6N_{1\mathrm{s}}^2 N_{1\mathrm{p}_0}^2 N_{1\mathrm{p}_1}^2 \bar{N}_{1\mathrm{p}_1}^2 + 8N_{1\mathrm{s}}^2 N_{1\mathrm{p}_0} \bar{N}_{1\mathrm{p}_0} N_{1\mathrm{p}_1}^3 \bar{N}_{1\mathrm{p}_1} \\ & + N_{1\mathrm{s}}^2 \bar{N}_{1\mathrm{p}_0}^2 N_{1\mathrm{p}_1}^4 + 8N_{1\mathrm{s}} \bar{N}_{1\mathrm{s}} N_{1\mathrm{p}_0}^2 N_{1\mathrm{p}_1}^3 \bar{N}_{1\mathrm{p}_1} \\ & + 4N_{1\mathrm{s}} \bar{N}_{1\mathrm{s}} N_{1\mathrm{p}_0} \bar{N}_{1\mathrm{p}_0} N_{1\mathrm{p}_1}^4 + \bar{N}_{1\mathrm{s}}^2 N_{1\mathrm{p}_0}^2 N_{1\mathrm{p}_1}^4 \\ & \vdots \end{aligned} \tag{7}$$

It is straightforward to extend these formulae to higher ionization probabilities, but higher correlations will then become increasingly important. In a mean field description, one should only expect reliable estimates for ionization numbers much smaller than the total electron number.

4 Ionization probabilities in cluster-ion collisions

As a typical example for cluster-ion collisions, we discuss the test case of Ar^{8+} on Na_9^+. The Ar^{8+} ion has a velocity of $v = 12.5$ to $50 a_0$/fs, which is between half and twice the electronic Fermi velocity v_{F} of Na. We consider a variety of impact parameters b, ranging from 10 to 40 a_0. The excitations become more violent the closer the collisions are.

4.1 Time evolution of the ionization probabilities

In Figure 1 we compare the time evolution of various key observables: the dipole signal $D(t) = \langle \hat{D} \rangle = \int_{\mathcal{V}} \mathrm{d}^3\mathbf{r}\, z\, n(\mathbf{r},t)$,

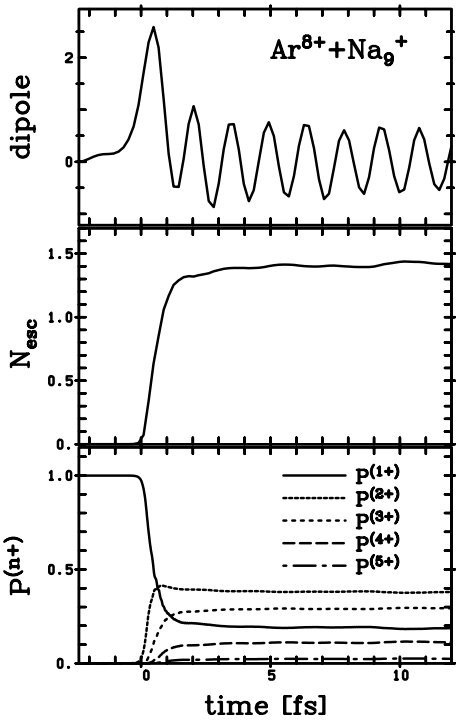

Fig. 1. Example of a typical response of the electron cloud for the collision of Ar^{8+} with velocity $v = 50\,a_0/\mathrm{fs} = 2\,v_\mathrm{F}$ on Na_9^+ at impact parameter $b = 22a_0$. We show the dipole moment (upper part), the total number of escaped electrons (middle part) and ionization probabilities $P^{(n+)}$ (lower part) as a function of time.

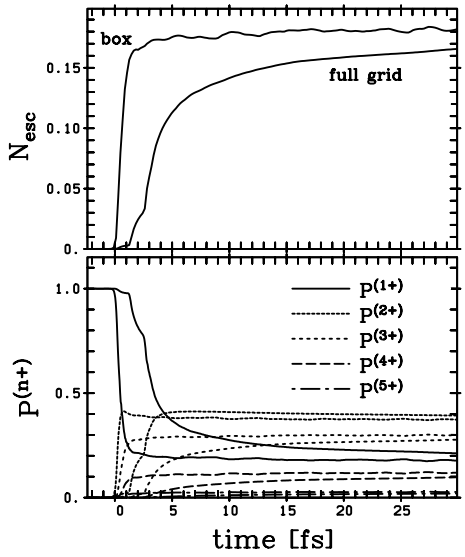

Fig. 2. Comparison of N_esc (upper panel, in fraction of total number of electrons) and ionization probabilities $P^{(n+)}$ (lower panel) as computed in the analyzing box *versus* the whole computational grid. The same line types are used for both cases. They are easily distinguished by the fact that results from the analyzing box start to change earlier and converge more rapidly. Kinematical conditions are the same as in Figure 1.

the number of escaping electrons $N_\mathrm{esc}(t)$, and the ionization probabilities. Results are shown for a typical test case with $v = 50\,a_0/\mathrm{fs} = 2\,v_\mathrm{F}$ and $b = 22\,a_0$. The Coulomb field (Eq. (1)) of the ion acts for an extremely short time, actually less than 1 fs. At the instant of closest approach ($t = 0$), we see a sudden change of the dynamical state of the system. The dipole oscillations are excited almost instantaneously, as can be seen in the uppermost panel of Figure 1. The subsequent electron emission follows immediately and is accomplished within the time of about one plasmon cycle (less than 2 fs), as can be seen from the number of escaped electrons N_esc in the middle panel. The ionization probabilities (lowest panel) are formed, of course, at the same fast time scale. The rapid loss of electrons causes a pronounced damping of the dipole oscillation in the earliest stage of the reaction. After that, the electron cloud oscillates steadily, while the ionization probabilities have stabilized at their asymptotic values. All competing processes follow at a slower pace: the internal damping of the dipole oscillations (Landau damping, electron-electron collisions) has characteristic times much larger than the dipole period itself [24]; charge-induced fission (involving ionic motion) [25] and thermal emission processes [26] occur far beyond 100 fs. They thus do not interfere with the much faster ionization induced by direct electron emission.

To compute the quantities presented in Figure 1, the density integrations have been performed over the analyzing box $\mathcal{V}$, as discussed in Section 3. It has been shown earlier that this is a reliable procedure, for the dipole moment of clusters [13] as well as for the number of electrons escaping atoms in strong fields [20–23], but we still have to check its validity for ionization probabilities and numbers of escaping electrons in the case of clusters. This is illustrated in Figure 2, where we have plotted both the number of escaping electrons and the ionization probabilities: i) computed in the analyzing volume $\mathcal{V}$ as defined in Section 3, and ii) computed from unrestricted integration over the whole volume of the numerical grid. The latter is about forty times larger than $\mathcal{V}$ and has absorbing boundaries. As one could have expected, the first steep increase of N_esc and $P^{(n+)}$ occurs with a delay of about 2 fs, if calculated on the total grid. This is related to the time which passes between the moment the ionized electrons cross the boundaries of the analyzing box until they completely leave the numerical grid. Moreover, N_esc and $P^{(n+)}$ rise more slowly on the total grid. This is related to the broad spectrum of velocities for the escaping electrons, which leads to a large variety of traveling times across the grid. But most important, all quantities approach asymptotically the values attained (earlier) in the analyzing box. Altogether, this comparison shows that, up to details of the time profile, electron emission is robustly and efficiently described within the analyzing box $\mathcal{V}$. We shall hence rely on this evaluation in the following.

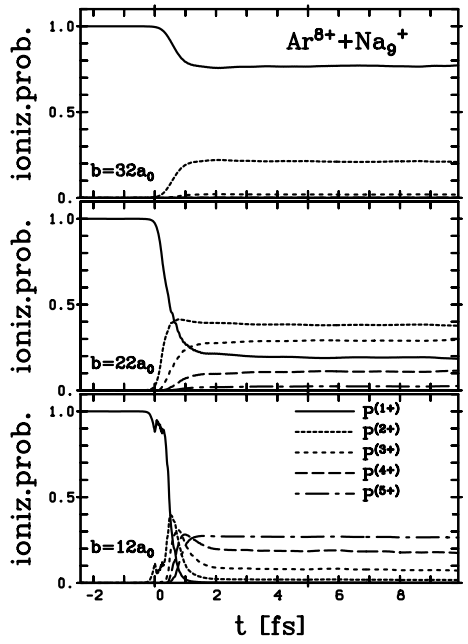

Fig. 3. Ionization probabilities $P^{(n+)}$ as function of time for the collision of Ar^{8+} with velocity $v = 50\,a_0/\mathrm{fs} = 2\,v_\mathrm{F}$ on Na_9^+. Results are shown for three different impact parameters b, as indicated.

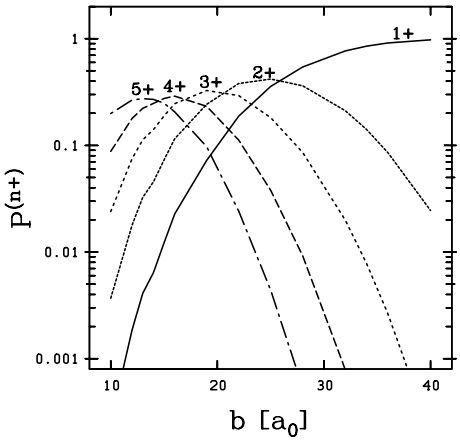

Fig. 4. The final ionization probabilities $P^{(n+)}(t = 12\,\mathrm{fs})$ as function of the impact parameter for the case of the velocity $v = 2\,v_\mathrm{F}$.

4.2 Dependence on the impact parameter

Variation of the impact parameter at fixed velocity allows us to change systematically the violence of the collision. The temporal pattern of excitation nevertheless remains the same, namely quasi-instantaneous dipole excitation and subsequent rapid electron emission, both occurring in less than 2 fs. However, differences show up in the amplitude of the dipole oscillations and in the number of emitted electrons, which both decrease with increasing impact parameter b. In Figure 3 we compare the time evolution of the ionization probabilities (see Sect. 3) at $v = 50\,a_0/\mathrm{fs} = 2\,v_\mathrm{F}$ for three different impact parameters: $b = 12$, 22 and $32\,a_0$. All cases evolve at the same time scale, but the distribution of ionization substantially changes. While the "asymptotic" probability decreases monotonically with increasing charge state for the largest impact parameter, $b = 32\,a_0$, the lowest charge state 1+ already falls below the next two higher states at $b = 22\,a_0$, and a complete turnover of the ordering has taken place at the smallest impact parameter $b = 12\,a_0$.

The situation becomes more transparent if the asymptotic values for the ionization probabilities are plotted *versus* impact parameter. We are taking here the values at $t = 12\,\mathrm{fs}$ where the emission processes have already converged, see Figure 3. The result is shown in Figure 4. The probability for the initial charge state 1+ decreases monotonically, as expected. For charge states $\geq 2+$, we see a rise and a fall of each ionization probability with decreasing b, such that the next higher charge state is following the previous one. The doubly ionized state appears first, with a maximum around $b = 25\,a_0$. It is followed by the triply ionized state which dominates around $b = 20\,a_0$, and so forth. The height of the maxima decreases slowly with growing charge. This is due to the fact that in this regime several different charge states coexist with comparable weight, and their probabilities must still sum up to unity. But in their region of dominance, even the higher charge states still attain peak probabilities of more than 0.25.

4.3 Ionization cross sections

Similar patterns for $P^{(n+)}$ *versus* b are observed at the lower ion velocities which we have considered. There is only a minimal shift of the maxima towards smaller b. The major differences lie in the absolute values of the asymptotic probabilities, with the tendency to increase with decreasing velocity. This means that more reaction time (allowed by lower velocities) enhances the ionization. To see the overall chances for obtaining a certain charge state $k > 1+$, one can look at the corresponding total production cross section σ^k, defined as

$$\sigma^k = 2\pi \int_0^\infty \mathrm{d}b\, b\, P^k(t \to \infty). \tag{8}$$

Results for the P^k are available for $10\,a_0 < b < 40\,a_0$, so that we have to restrict the integration in equation (8) to this interval. This means that we obtain in fact lower bounds to the σ^k. On the other hand, from Figure 4 we also see that, at least for the charge states 2+ through 5+, the probabilities have their maximum in the considered range of b and decrease sharply for smaller/larger values of b. In addition to this, note that the significance of the P^k for smaller values of b is strongly reduced, due to the weight factor b in the integral in equation (8). It is thus a good approximation to neglect their contributions to σ^k for $b < 10\,a_0$, even in the lower velocity cases ($v = 0.5 v_\mathrm{F}$ and $v = v_\mathrm{F}$), in which the maxima are slightly shifted

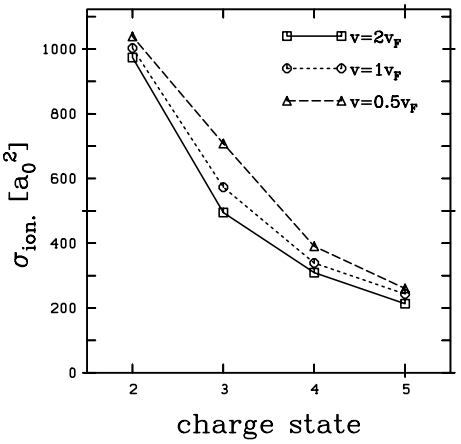

Fig. 5. The total ionization cross sections for the various final charge states and for different velocities, as indicated.

to smaller values. This, actually, would mainly affect the highest charge states.

The resulting σ^k are shown in Figure 5, for three different velocities at and around $v_{\rm F}$. The cross sections decrease with increasing charge state, but the decrease is slow enough so that higher charge states still acquire appreciable values. For example, the production of charge state 5+ has a cross section of at least 6×10^9 barn. One also notes that for a given charge state the cross section decreases with increasing projectile velocity. The effect is largest for charge state 3+ (almost a factor 2 between $v = 0.5v_{\rm F}$ and $v = 2v_{\rm F}$) and less pronounced for the higher charge states 4+ and 5+. To summarize, we see that collisions with fast ions with velocities in the electronic Fermi velocity range can be used as an efficient method to produce highly ionized states of a cluster.

5 Trapping versus direct emission

The nature of the ionization process deserves further inspection. Two different mechanisms are conceivable. First, the Coulomb potential of the ion can suppress the potential barrier of the cluster so that the electrons at the Fermi level can immediately flow into the Coulomb field of the ion and are most likely *trapped* in its attractive potential. And second, the Coulomb force of the rapidly by-passing ion transfers almost instantaneously a certain amount of momentum to the electron cloud, which triggers a pronounced collective oscillation. The oscillating electron cloud then immediately emits its content of continuum electrons within the first few cycles; we call this *direct* emission [14]. It is obvious that the relative weight of these competing mechanisms depends on the reaction time, *i.e.* on the ion velocity. Well below the Fermi velocity ($v \sim v_{\rm F}/10$), the contact time becomes long enough for an efficient barrier suppression, and we expect trapping to become relevant. Direct emission will become the dominating process for $v \sim v_{\rm F}$. Let us now consider this ionization mechanism in more detail in the high velocity case.

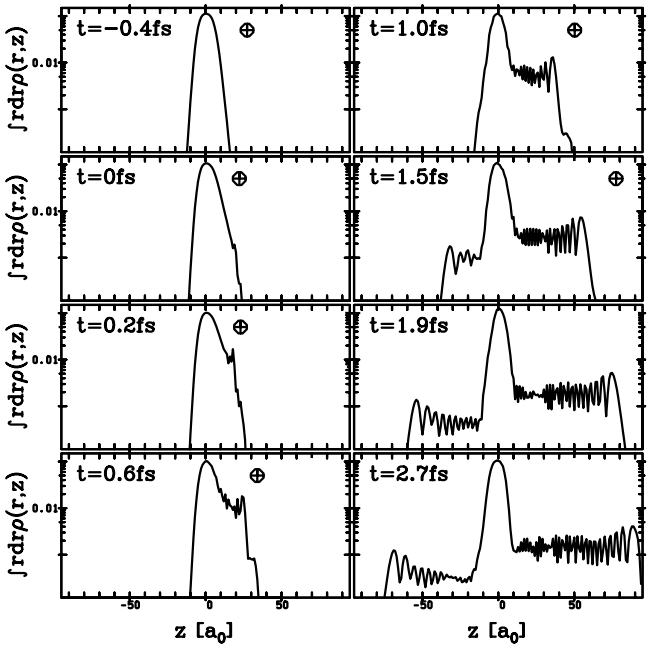

Fig. 6. Snapshots of the electron density for the case $v = 2\,v_{\rm F}$ and $b = 22\,a_0$ at various stages at and shortly after the time of closest approach of the ion. The ionic position is indicated by a circled cross, at each considered instant. The density (integrated over the radial and angular coordinates) is drawn along the symmetry axis (z-axis). Note that a logarithmic scale is used for the density in order to display more clearly the processes in the tail of the distribution.

5.1 A visual analysis of trapping

In order to disentangle both mechanisms, direct emission *versus* trapping, we have to investigate the emission process in more detail. This is most conveniently done by looking at snapshots of the density profile at different times. In practice, we display the density along the z-axis, averaged over the radial direction. The example of a high velocity collision with $v = 2v_{\rm F}$ and intermediate impact parameter $b = 22\ a_0$ is shown in Figure 6. As the ion comes close to the cluster, we see that the electron cloud is gradually deformed towards the ion. However, there is not particularly much electron density gathered directly at the ion, neither at contact time nor in the subsequent time steps (note the logarithmic scale for the density). At best, a long electron tail stretches out between the ion and the cluster. The ion moves too fast away for the cloud to follow and leaves this scenario virtually naked. It is interesting to see a much similar electron wing extending in exactly the opposite direction with about half a plasmon cycle delay. This confirms the picture that, in this case of high ion velocity, we are seeing predominantly a plasmon oscillation shaking off its continuum electrons at every turning point. The effect is of course most pronounced

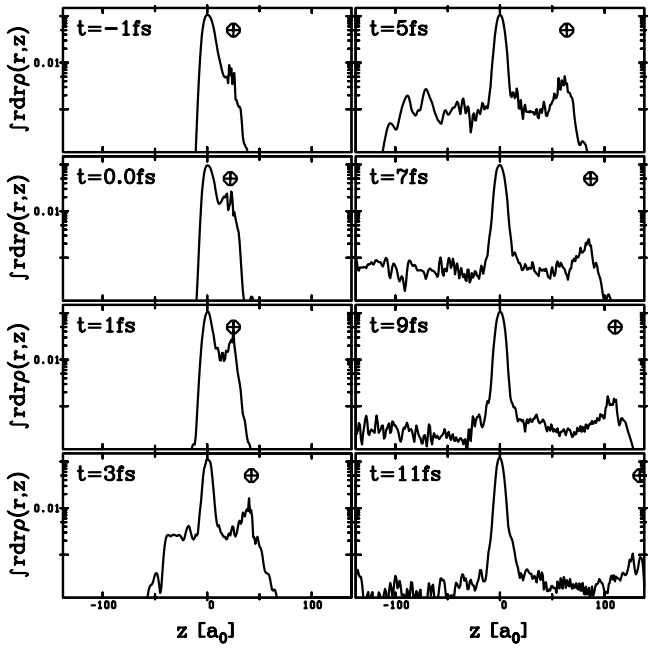

Fig. 7. Same as Figure 6, but for $v = 0.5\,v_{\rm F}$ and $b = 22\,a_0$.

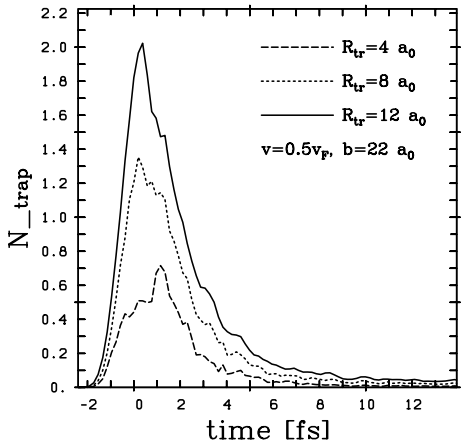

Fig. 8. Number of electrons trapped in the vicinity of Ar^{8+} as a function of time, analyzed in spherical volumes around the ion, using three different radii as indicated. The Ar^{8+} ion is passing by the $Na_9{}^+$ cluster with velocity $v = 0.5\,v_{\rm F}$ and impact parameter $b = 22\,a_0$.

at the first turning point, with the outgoing electron flux directed towards the ion, because the exciting Coulomb pulse is attractive. Thus we can conclude that we see almost exclusively *direct* emission in this test case. We have counterchecked this by comparing with an excitation by a pure instantaneous initial dipole shift leading to the same average excitation energy. The emission pattern looks very similar to the one shown in Figure 6, and the resulting ionization probabilities are also in quantitative agreement. To complete the reasoning, we have also looked at two other impact parameters, $b = 12$ and $32\,a_0$, and found the same predominance of direct emission.

As discussed above, the scenario is expected to change with lower velocity. We thus explore a test case with $v = 0.5v_{\rm F}$, again at the intermediate impact parameter $b = 22\,a_0$. The corresponding density snapshots are displayed in Figure 7 (note the different time and length scales as compared to Fig. 6). The overall picture is qualitatively similar to the higher energy case, in particular concerning the role of the plasmon in "shaking off" the continuum electrons. Still, the lower projectile velocity allows the electron cloud to follow the projectile more closely, as one can see from the small density peak which is always found near the ion. Although the general level and pattern of emitted density remain comparable to the high energy case, one may expect that this density peak following the ion will eventually result in a larger number of trapped electrons. We shall now analyze this in a more quantitative manner.

5.2 An estimate of the number of trapped electrons

The simplest way to analyze the number of trapped electrons is to integrate the electron density in a spherical box with radius $R_{\rm tr}$ around the projectile. We thus define the number of trapped electrons by

$$N_{\rm trap}(R_{\rm tr};t) = \int {\rm d}^3\mathbf{r}\, n(\mathbf{r},t)\theta(R_{\rm tr} - |\mathbf{r} - \mathbf{R}_{\rm ion}(t)|), \quad (9)$$

where $\mathbf{R}_{\rm ion}(t)$ indicates the position of the ion, and $\theta(x) = 1$ for $x > 0$ and 0 for $x < 0$. There is some arbitrariness in choosing the trapping radius $R_{\rm tr}$. A small $R_{\rm tr}$ will confine the analysis to deeply bound states, while a very large one allows for loose trapping. We therefore consider three different choices: $R_{\rm tr} = r_{\rm s}$, $2r_{\rm s}$ and $3r_{\rm s}$ (where we have taken $r_{\rm s} = 4a_0$ in sodium). Furthermore, following the time evolution of $N_{\rm trap}(R_{\rm tr};t)$ allows one to investigate the stability of the trapping. In Figure 8 we show $N_{\rm trap}(R_{\rm tr};t)$ as a function of time for the impact parameter $b = 22\,a_0$ and projectile velocity $v = 0.5v_{\rm F}$, which favours trapping (Sect. 5.1). The number of trapped electrons of course increases with $R_{\rm tr}$, but the time profiles of the three curves are very similar. They display a pronounced peak at the time of closest approach (around $t = 0$) with a large number of temporarily attached electrons (up to 2 for the highest value of $R_{\rm tr}$). The number of trapped electrons then quickly decreases again and stabilizes towards an asymptotic value of a small fraction of an electron (less than 0.05). The initial accumulation of electron density around the projectile thus quickly dissolves, indicating that the electrons are in fact not truly trapped by the projectile potential well. They do not even seem to remain in a loose vicinity of the projectile, as indicated by the results for the largest $R_{\rm tr}$.

It should be noted that, although this electron "dispersal" takes place on a short time scale (of less than 10 fs), it is technically demanding to ascertain it, because of the high projectile velocity. Indeed, at $v = 0.5v_{\rm F}$, the projectile travels at $12.5\,a_0$ per fs, which means that at t=14 fs (Fig. 8), it is at a distance $d \sim 180\,a_0$ away from the cluster's center of mass. It hence requires a huge

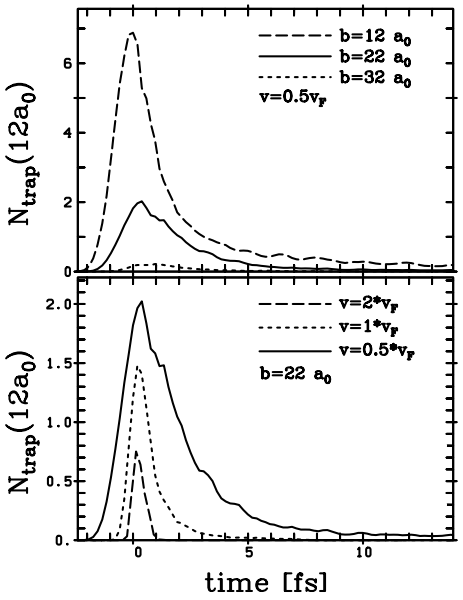

Fig. 9. Number of electrons trapped in the vicinity of Ar^{8+} ($R_{\rm tr} = 12\,a_0$) as a function of time, for various impact parameters at fixed velocity $v = 0.5\,v_{\rm F}$ (upper panel) and for various ion velocities at fixed impact parameter $b = 22\,{\rm a}_0$ (lower panel).

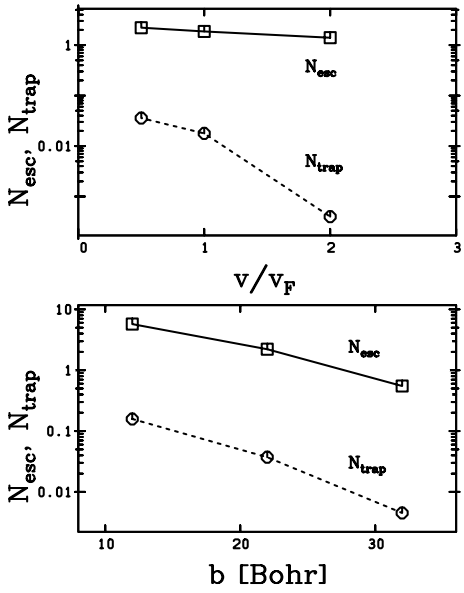

Fig. 10. Asymptotic numbers of escaped electrons, $N_{\rm esc}$, and of electrons trapped in a $12\,a_0$ vicinity of Ar^{8+}, $N_{\rm trap}$, for various ion velocities at fixed impact parameter $b = 22\,{\rm a}_0$ (upper part), and for various impact parameters at fixed ion velocity $v = 0.5\,v_F$ (lower part).

computational grid ($400\,a_0$ along z direction in our test case) to identify a plateau in $N_{\rm trap}$ and thus to pin down an asymptotic value for trapping. A computation in a small box ($50\,a_0$ for example, as typically chosen in a full 3D calculation [27]) would have to stop at $t = 4$ fs, leading to a totally erroneous value of $N_{\rm trap} \sim 0.4$.

5.3 Influence of projectile velocity and impact parameter

As discussed in Section 5.2, the evaluation of $N_{\rm trap}$ according to equation (9) provides a simple measure of the number of trapped electrons. In view of the small asymptotic values of $N_{\rm trap}$ shown in Figure 8, it is sufficient to continue our analysis with the largest box radius $R_{\rm tr} = 12\,a_0$. Figure 9 shows $N_{\rm trap}(R_{\rm tr} = 12\,a_0; t)$ for various impact parameters b at fixed $v = 0.5\,v_{\rm F}$ (upper panel) and various velocities v at fixed $b = 22\,a_0$ (lower panel). All curves display the same pattern, as discussed in Section 5.2: a short attachement of a possibly large number of electrons, followed within less than about 5 fs by a decrease to a very small value of $N_{\rm trap}$ (at most 0.2 for the most favourable case, with $v = 0.5v_{\rm F}$, and $b = 12\,a_0$). We can thus conclude that, in the energy and velocity range under consideration, one never observes large asymptotic values of electron trapping. A possibly large number of electrons may be attached initially, but this lasts only for a short time: sizable trapping is unstable.

It is finally interesting to summarize our findings by plotting the asymptotic values $N_{\rm trap}(t = 12 - 14\,{\rm fs})$ as a function of the projectile velocities and impact parameters, and to compare $N_{\rm trap}$ to the total number of escaped electrons $N_{\rm esc}$ (which is also stabilized at that time). This comparison is performed in Figure 10. While $N_{\rm esc}$ may reach sizable values, in particular at low velocity (up to 5-6 at $b = 12a_0$ for $v = 0.5v_{\rm F}$), $N_{\rm trap}$ never exceeds 0.2, and becomes more and more negligible with respect to $N_{\rm esc}$, the larger the impact parameter or the projectile velocity. Altogether, we find that $0.3\% \leq N_{\rm trap}/N_{\rm esc} \leq 4\%$), which clearly shows that trapping is negligible as compared to direct emission in the kinematic range we consider here.

6 Conclusion

We have investigated electron emission from a metal cluster following excitation by a fast and highly charged ion passing by. The actual test case was Ar^{8+} colliding with Na_9^+ at velocities between half and twice the electronic Fermi velocity of Na and various impact parameters, from grazing to very peripheral collisions. As theoretical tool for the dynamics of the electron cloud of the cluster we used the TDLDA. In particular, we have been concerned with the ionization probabilities deduced from the occupation numbers of the time-dependent single-particle orbitals. We find sizable ionization probabilities and cross sections for producing high charge states of the cluster. The excitation process as such proceeds at a very fast time scale of clearly less than one plasmon cycle. The subsequent electron emission and the way to the final ionization probabilities is also extremely fast, taking only about one plasmon cycle. Moreover, in the kinematic regime we have considered here, we find that the excitation is so short that virtually no trapping takes place. Direct emission following

the instantaneous dipole excitation of the electron cloud is thus the predominant mechanism. The short time scales involved and the dominance of direct emission leave the ionic background almost completely undisturbed during the reaction and thus make energetic ion impact a very clean excitation process well suited for studies of cluster dynamics in highly ionized states.

The authors thank the French-German exchange program PROCOPE 95073 and the Institut Universitaire de France for financial support during the realization of this work.

References

1. U. Näher, S. Björnholm, S. Frauendorf, F. Garcias, C. Guet, Phys. Rep. **285**, 245 (1997).
2. C. Bréchignac, P. Cahuzac, F. Carlier, M. de Frutos, Phys. Rev. Lett. **64**, 2893 (1990); C. Bréchignac, P. Cahuzac, F. Carlier, M. de Frutos, R.N. Barnett, U. Landmann, Phys. Rev. Lett. **72**, 1636 (1994).
3. U. Näher, H. Göhlich, T. Lange, T.P. Martin, Phys. Rev. Lett. **68**, 3416 (1992); U. Näher, S. Frank, N. Malinowski, U. Zimmermann, T.P. Martin, Z. Phys. D **31**, 191 (1994).
4. F. Chandezon, C. Guet, B.A. Huber, D. Jalabert, M. Maurel, E. Monnand, C. Ristori, J.C. Rocco, Phys. Rev. Lett. **74**, 3784 (1995).
5. P.A.M. Dirac, Proc. Camb. Phil. Soc. **26**, 376 (1930).
6. E.K.U. Gross, W. Kohn, Adv. Quant. Chem. **21**, 255 (1990).
7. E.K.U. Gross, C.A. Ullrich, U.J. Gossmann, in *Density Functional Theory*, edited by E.K.U. Gross and R.M. Dreizler, NATO ASI series B337 (Plenum Press, New York, 1994).
8. E.K.U. Gross, J.F. Dobson, M. Petersilka, in *Density Functional Theory II*, Vol. 181 of *Topics in Current Chemistry*, edited by R.F. Nalewajski (Springer, Berlin, 1996), p. 81.
9. M. Gross, C. Guet, Z. Phys. D **33**, 289 (1995).
10. L. Féret, E. Suraud, F. Calvayrac, P.-G. Reinhard, J. Phys. B **29**, 4477 (1996).
11. F. Calvayrac, P.G. Reinhard, E. Suraud, Phys. Rev. B **52**, R17056 (1995).
12. L. Mornas, F. Calvayrac, E. Suraud, P.-G. Reinhard, Z. Phys. D **38**, 81 (1996).
13. F. Calvayrac, P.-G. Reinhard, E. Suraud, Ann. Phys. (N.Y.) **255** 125 (1997).
14. C.A. Ullrich, E. Suraud, P.-G. Reinhard, Phys. Rev. A (to be published).
15. C.A. Ullrich, A. Domps, F. Calvayrac, E. Suraud, P.-G. Reinhard, Z. Phys. D **40**, 265 (1997).
16. C.A. Ullrich, P.-G. Reinhard, E. Suraud, J. Phys. B: At. Mol. Opt. Phys. **30**, 5043 (1997).
17. A. Rubio, L.C. Balbas, J.A. Alonso, Z. Phys. D **19**, 93 (1991).
18. P.-G. Reinhard, O. Genzken, M. Brack, Ann. Phys. (Leipzig) **5**, 576 (1996).
19. O. Gunnarsson, B.I. Lundqvist, Phys. Rev. B **13**, 4274 (1976).
20. C.A. Ullrich, S. Erhard, E.K.U. Gross, in *Super-Intense Laser-Atom Physics IV*, edited by H.G. Muller and M.V. Fedorov (Kluwer, Dordrecht, 1996); C.A. Ullrich, E.K.U. Gross, Comm. At. Mol. Phys. **33**, 211 (1997).
21. M. Horbatsch, H.J. Lüdde, R.M. Dreizler, J. Phys. B **25**, 3315 (1992).
22. K.C. Kulander, K.J. Schafer, J.L. Krause, in *Atoms in Intense Laser Fields*, edited by M. Gavrila (Academic Press, Boston, 1992).
23. M. Protopapas, C.H. Keitel, P.L. Knight, Rep. Prog. Phys. **60**, 389 (1997).
24. M. Brack, Rev. Mod. Phys. **65**, 677 (1993).
25. R.N. Barnett, U. Landmann, G. Rajagopal, Phys. Rev. Lett. **67**, 3058 (1991).
26. V. Weisskopf, Phys. Rev. **52**, 295 (1937).
27. P.-G. Reinhard, J. Babst, B. Fischer, C. Kohl, F. Calvayrac, E. Suraud, T. Hisrchmann, M. Brack, Z. Phys. D **40**, 314 (1997).